The short-chain fatty acid acetate coordinates with CD30 to modulate T-cell survival

Junfang Lyu[a,b], Ziyi Li[c], Jessica P. Roberts[c], Yue A. Qi[c], and Jianhua Xiong[a,b,*]
[a]Department of Medicine, Division of Endocrinology, Diabetes and Metabolism, Johns Hopkins University School of Medicine, St. Petersburg, FL 33701; [b]Institute for Fundamental Biomedical Research, Johns Hopkins All Children's Hospital, St. Petersburg, FL 33701; [c]Center for Alzheimer's and Related Dementias (CARD), National Institute on Aging and National Institute of Neurological Disorders and Stroke, National Institutes of Health, Bethesda, MD 20892

ABSTRACT **As an important substrate for cell metabolism, the short-chain fatty acid acetate emerges as a regulator of cell fate and function. However, its role in T-cell survival and its underlying mechanisms remain largely unknown. Here, we demonstrate that acetate modulates T-cell apoptosis via potentiation of α-tubulin acetylation. We further show that acetate treatment effectively increases the expression of the tumor necrosis factor receptor (TNFR) family member CD30 by enhancing its gene transcription. Moreover, CD30 physically associates with and stabilizes the deacetylase HDAC6, which deacetylates α-tubulin to decrease microtubule stability. Proteomic profiling of CD30 knockout (*Cd30*$^{-/-}$) T-cells reveals elevated expression of anti-apoptotic BCL2 family proteins and thus promotes T-cell survival via a microtubule-Bcl-2 axis. Taken together, our results demonstrate that acetate is a regulator of T-cell survival by controlling levels of acetylated α-tubulin. This suggests that therapeutic manipulation of acetate metabolism may facilitate optimal T-cell responses in pathological conditions.**

Monitoring Editor
Avery August
Cornell University

Received: Jan 30, 2023
Revised: Apr 28, 2023
Accepted: May 1, 2023

INTRODUCTION

There is a growing appreciation that cellular metabolism instructs and modulates T-cell differentiation and function at multiple levels (Geltink *et al.*, 2018). The lives and deaths of T-cells are highly dynamic and tightly regulated and are accompanied by significant metabolic rewiring (Bantug *et al.*, 2018). Many observations collectively support the importance of metabolic and interlinked signaling requirements for both T-cell fate decision and function, as well as T-cell survival and homeostasis (Jung *et al.*, 2019). Interestingly, several lines of evidence suggest that the short-chain fatty acid acetate is a critical metabolic mediator of T-cell fate and function (Balmer *et al.*, 2016; Peng *et al.*, 2016; Hu *et al.*, 2019; Qiu *et al.*, 2019). For instance, acetate can rescue CD8$^+$ T-cell effector function during glucose restriction (Qiu *et al.*, 2019). In another report, low maternal serum acetate impairs the development of fetal thymic regulatory T-cells in the pregnancy-associated disorder preeclampsia (Hu *et al.*, 2019). In contrast, a systemic increase in serum acetate levels following bacterial infection is required for optimal rapid recall responses and function of memory CD8$^+$ T-cells (Balmer *et al.*, 2016). Even though acetate appears to have a significant impact on T-cell fate determination and function, its precise role and the molecular mechanisms by which it regulates T-cell survival and homeostasis are poorly understood.

Acetate is converted into acetyl-coenzyme A (acetyl-CoA) through the action of acyl-CoA synthetase short-chain family member 2 (ACSS2; Moffett *et al.*, 2020). Metabolically, acetyl CoA is positioned as a major central metabolite that is key both to catabolic processes required for energy production and to anabolic pathways that drive macromolecular biosynthesis (Pietrocola *et al.*, 2015; Xiong, 2018a, 2018b). Acetyl CoA is also the sole donor of the acetyl groups for the acetylation of key lysines and arginines of many proteins that modulate their roles in a wide variety of cellular signaling pathways and biological processes (Cai *et al.*, 2011; Lee *et al.*, 2014). Mounting evidence suggests that supplementation of cells with the acetyl-CoA precursor acetate can affect gene expression,

This article was published online ahead of print in MBoC in Press (http://www.molbiolcell.org/cgi/doi/10.1091/mbc.E23-01-0032) on May 10, 2023.

*Address correspondence to: Jianhua Xiong (jxiong10@jhmi.edu).

Abbreviations used: Acetyl CoA, acetyl coenzyme A; ACSS2, acyl coenzyme A synthetase short-chain family member 2; Bcl-2, B-cell lymphoma 2; *Cd30*$^{-/-}$, CD30 knockout; ChIP–qPCR, chromatin immunoprecipitation quantitative real-time PCR; co-IP, coimmunoprecipitation; H3K27ac, histone H3 acetylation at lysine 27; KEGG, *Kyoto Encyclopedia of Genes and Genomes*; TNFR, tumor necrosis factor receptor; WT, wild type.

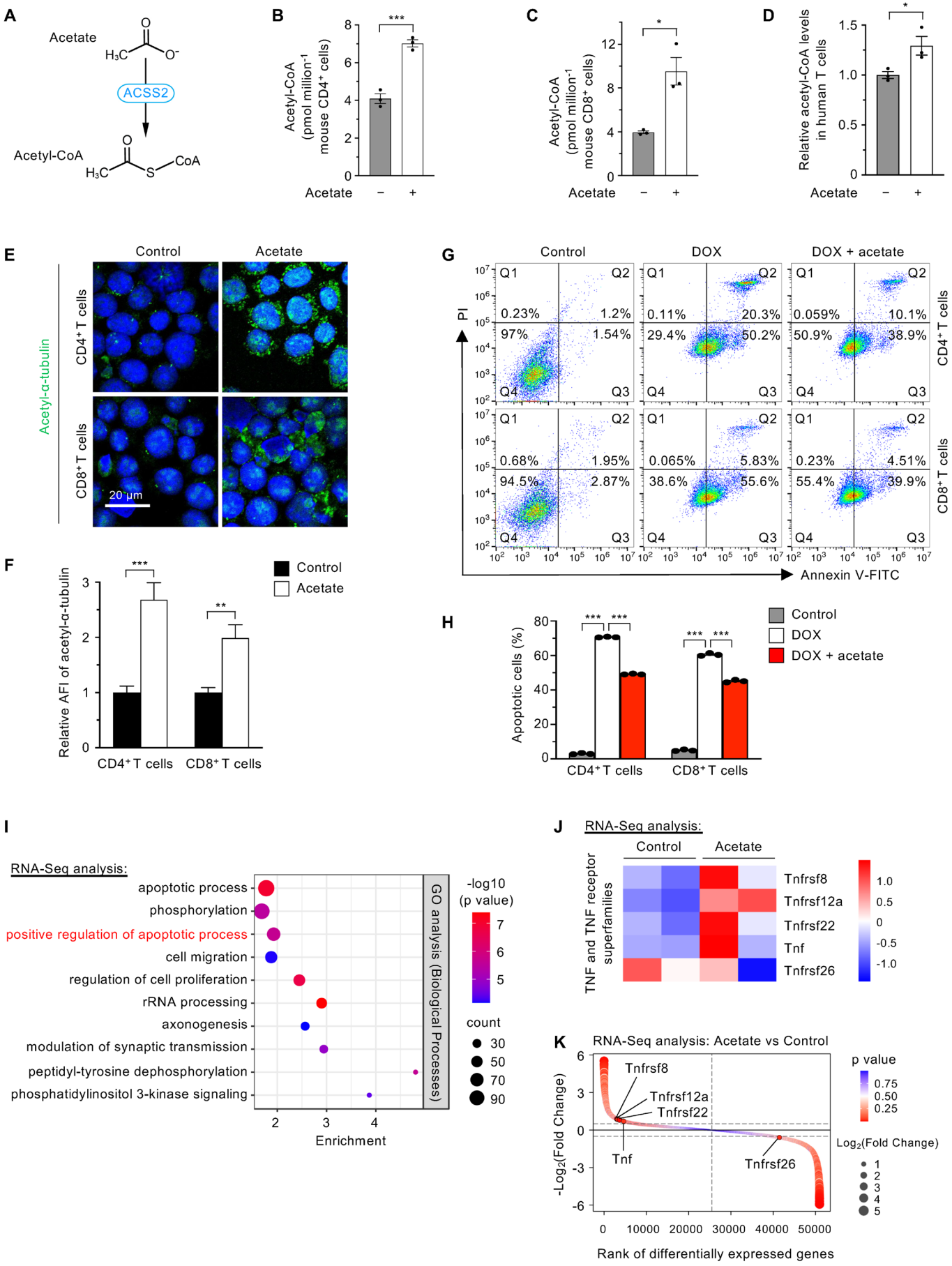
A
Acetate
ACSS2
Acetyl-CoA
CoA
B
Acety-CoA (pmol million-1 mouse CD4+ cells)
Acetate
C
Acetyl-CoA (pmol million-1 mouse CD8+ cells)
D
Relative acetyl-CoA levels in human T cells
E
Control
Acetate
Acetyl-α-tubulin
CD4+ T cells
CD8+ T cells
20 μm
F
Relative AFI of acetyl-α-tubulin
Control
Acetate
CD4+ T cells
CD8+ T cells
G
Control
DOX
DOX + acetate
PI
Annexin V-FITC
Q1
Q2
Q3
Q4
0.23%
1.2%
97%
1.54%
0.11%
20.3%
29.4%
50.2%
0.059%
10.1%
50.9%
38.9%
0.68%
1.95%
94.5%
2.87%
0.065%
5.83%
38.6%
55.6%
0.23%
4.51%
55.4%
39.9%
H
Apoptotic cells (%)
Control
DOX
DOX + acetate
I
RNA-Seq analysis:
apoptotic process
phosphorylation
positive regulation of apoptotic process
cell migration
regulation of cell proliferation
rRNA processing
axonogenesis
modulation of synaptic transmission
peptidyl-tyrosine dephosphorylation
phosphatidylinositol 3-kinase signaling
Enrichment
GO analysis (Biological Processes)
-log10 (p value)
count
J
RNA-Seq analysis:
Control
Acetate
TNF and TNF receptor superfamilies
Tnfrsf8
Tnfrsf12a
Tnfrsf22
Tnf
Tnfrsf26
K
RNA-Seq analysis: Acetate vs Control
-Log2(Fold Change)
p value
Log2(Fold Change)
Rank of differentially expressed genes

protein stability, and cell fate and function by directly increasing acetyl-CoA levels, which in turn increases protein acetylation (Schug *et al.*, 2015; Balmer *et al.*, 2016; Wong *et al.*, 2017; Xiong *et al.*, 2018; Lyu *et al.*, 2022).

We first examined how acetate inhibits T-cell apoptosis through acetylation of α-tubulin, and then explored the role of acetate in potentiating the expression of CD30 in T-cells, specifically whether CD30 modulates acetate-associated α-tubulin acetylation and microtubule stability. Finally, we investigated how acetate coordinates with CD30 to modulate T-cell survival via a microtubule-Bcl-2 signaling axis.

RESULTS AND DISCUSSION

Acetate inhibits T-cell apoptosis through acetylation of α-tubulin

To examine the effects of acetate on T-cell apoptosis, we took advantage of recent observations that acetate supplementation in cell culture can directly increase acetyl-CoA levels through the action of ACSS2 (Figure 1A; Balmer *et al.*, 2016; Schug *et al.*, 2015). We supplemented the culture media in both mouse and human T cells with acetate and found an increase in acetyl-CoA levels (Figure 1, B–D). In accordance with a posttranslational mechanism, we reasoned that increasing acetyl-CoA levels by exogenous acetate supplementation might modulate protein acetylation in T-cells.

There is increasing evidence that α-tubulin acetylation stabilizes microtubules (Gu *et al.*, 2016; Lyu *et al.*, 2022), and it is known that deregulated microtubule dynamics and stability lead to apoptosis (Mollinedo and Gajate, 2003; Knipling and Wolff, 2006). Therefore, we hypothesized that acetate might modulate T-cell apoptosis by contributing to the acetylation of α-tubulin and microtubule instability. We found that acetate supplementation robustly enhanced the levels of α-tubulin acetylation in T-cells (Figure 1, E and F). Furthermore, consistent with an earlier report (Gamen *et al.*, 1997), we found that acetate supplementation promoted α-tubulin acetylation and that this inhibited doxorubicin-induced T-cell apoptosis, as evidenced by a decrease in the apoptosis marker cleaved caspase-3 levels (Supplemental Figure S1A). We obtained similar results using the annexin V staining method (Figure 1, G and H). To further assess whether the levels of acetylated α-tubulin play a role in doxorubicin-induced apoptosis, we took advantage of the acetylation-resistant tubulin mutant K40R (Gao *et al.*, 2010). Although the flag-tagged K40R mutant appears to have no effects on the endogenous acetylated α-tubulin levels, the acetate-mediated total acetylated α-tubulin levels (sum of the flag-tagged and endogenous acetylated α-tubulin levels) were reduced in cells with K40R mutant compared with those with flag-tagged wild-type (WT) α-tubulin (Supplemental Figure S1, B and C). We found that increasing total acetylated α-tubulin levels via acetate supplementation in cells with flag-tagged WT α-tubulin suppresses doxorubicin-induced cell apoptosis, while reducing total acetylated α-tubulin levels via use of the flag-tagged K40R mutant compromised the inhibitory effects of acetate on apoptosis (Supplemental Figure S1, B and C). Together, these results suggest that acetylated α-tubulin levels negatively regulate doxorubicin-induced cell apoptosis (Supplemental Figure S1, B and C). Although our data suggest that acetate negatively modulates T-cell apoptosis, possibly by regulating α-tubulin acetylation and microtubule stability, the detailed mechanisms underlying this regulation were unclear.

To gain further mechanistic insights into acetate-mediated negative regulation of T-cell apoptosis, we performed a transcriptomic profile using mouse $CD8^+$ T-cells cultured with and without acetate treatment (Supplemental Table S1). Unexpectedly, our gene ontology (GO) analysis pinpointed a significant change for the category "positive regulation of apoptosis process" (Figure 1I). Among all the differentially expressed genes within this category, the TNF and TNFR superfamily members showed signs of being highly enriched (Supplemental Figure S1D). TNF and TNFR superfamily proteins are known to play a central role in cell survival (Croft *et al.*, 2013). It has been shown that CD30 deficiency has an inhibitory effect on anti-CD3-mediated activation-induced death of thymocytes (Amakawa *et al.*, 1996). Our RNA-sequencing (RNA-Seq) analysis demonstrated that the CD30-encoding gene *Tnfrsf8* was significantly up-regulated by acetate (Figure 1, J and K), suggesting a potential role for CD30 in the positive regulation of apoptosis downstream from acetate signaling.

Acetate potentiates the expression of CD30 in T-cells

CD30 was initially identified as a cell surface maker expressed by the neoplastic Reed-Sternberg cells in Hodgkin's disease (Stein *et al.*, 1982). Subsequent studies have shown that CD30 expression exists not only in malignant cells, but also in a small subset of activated normal lymphocytes, including T-cells (van der Weyden *et al.*, 2017). Because our RNA-Seq analysis revealed that acetate is a potential inducer of CD30 gene expression (Figure 1, I and J), we next asked whether acetate is a bona fide regulator of CD30 expression in T-cells. We found that transcriptional levels of CD30 were markedly elevated by acetate in both mouse $CD4^+$ and $CD8^+$ T-cells, as measured by real-time quantitative reverse transcription PCR (qPCR) (Figure 2, A and B; Supplemental Figure S1, E and F).

To investigate how acetate controls CD30 gene transcription, we considered recent observations that found that acetate enhances transcription of specific cytokine genes by increasing the levels of histone H3 acetylation at lysine 27 (H3K27ac) at their promoter regions (Kendrick *et al.*, 2010; Qiu *et al.*, 2019). We treated mouse $CD4^+$ and $CD8^+$ T-cells with acetate and found elevated levels of total H3K27ac (Figure 2, C and D). H3K27ac marks transcriptionally active DNA and is predominantly found in active chromatin regions, including promoters (Matharu and Ahituv, 2020). Based on this concept, acetate supplementation facilitated chromatin accessibility

FIGURE 1: Acetate modulates T cell apoptosis through acetylation of α-tubulin. (A) ACSS2-mediated acetate conversion increases cytosolic acetyl CoA levels. (B–D) Levels of acetyl CoA in control or acetate-treated mouse $CD4^+$, B, and $CD8^+$, C, T-cells and human T-cells, D ($n = 3$ independent experiments). (E, F) Representative immunostaining images, E, and quantification, F, of acetyl α-tubulin in mouse T-cells with or without acetate treatment ($n = 10$ cells). (G, H) Flow cytometric analysis, G, and quantification, H, of cell apoptosis in mouse T-cells treated or not treated with doxorubicin (DOX) and treated or not treated with acetate ($n = 3$ independent experiments). (I) RNA-Seq bubble plot depicting top enriched GO biological processes for the differentially expressed genes in mouse $CD8^+$ T-cells treated or not treated with acetate ($n = 2$ biological replicates). (J) Heat map of RNA-Seq data for TNF and TNFR family genes within the GO category "positive regulation of apoptotic process" for the differentially expressed genes in mouse $CD8^+$ T-cells treated or not treated with ($n = 2$ biological replicates). (K) Fold change–based ranking of all genes differentially expressed in mouse $CD8^+$ T-cells treated or not treated with acetate ($n = 2$ biological replicates).

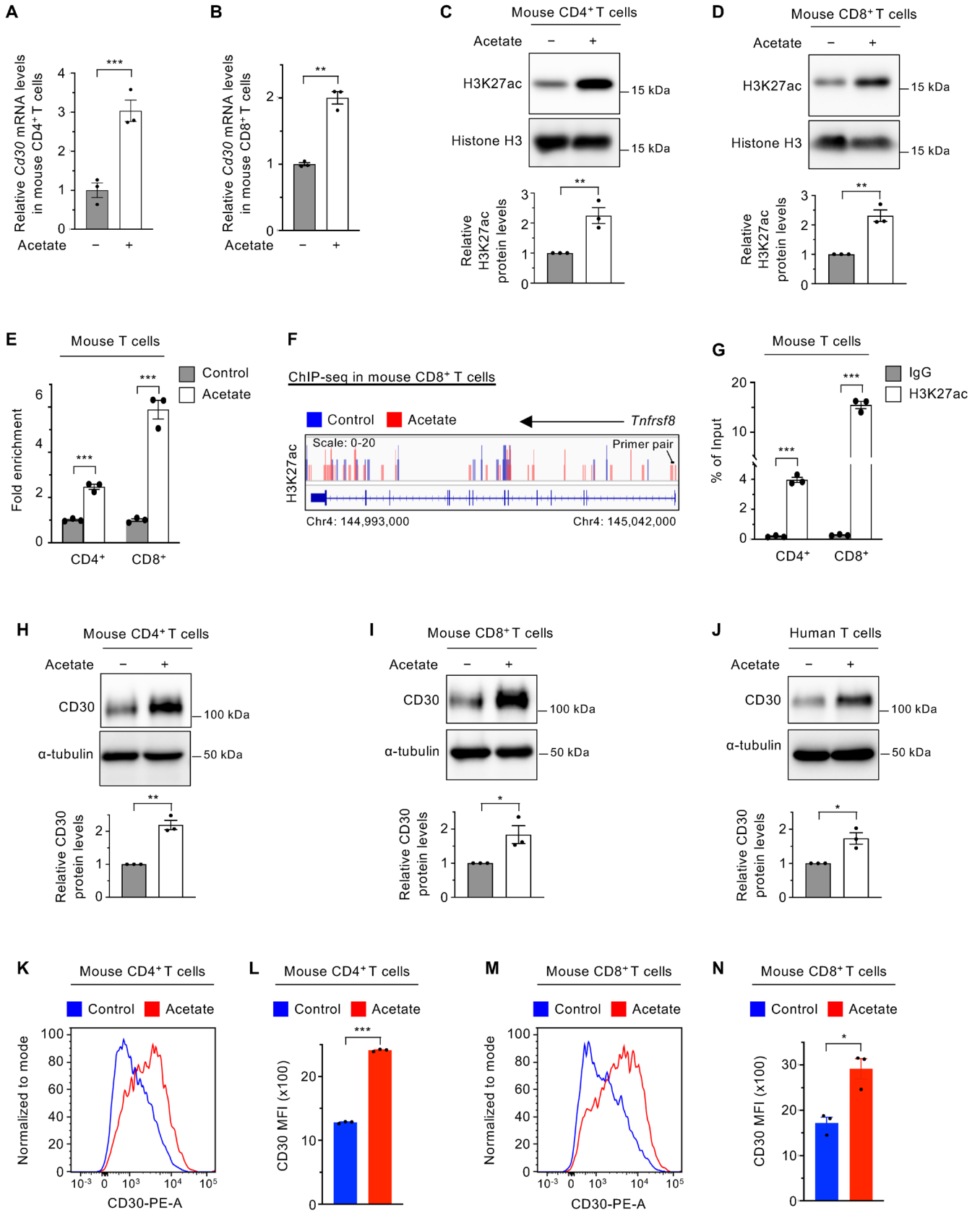

FIGURE 2: Acetate up-regulates CD30 expression in T-cells. (A, B) qPCR analysis of *Cd30* mRNA expression in mouse CD4+, A, and CD8+, B, T-cells with or without acetate treatment (technical triplicates per condition; data represent one of two independent experiments). (C, D) Western blot of H3K27ac in mouse CD4+, C, and CD8+, D, T-cells with or without acetate treatment ($n = 3$ independent experiments). (E) Chromatin accessibility analysis of the locus of CD30-encoding gene *Tnfrsf8* in mouse T-cells with or without acetate treatment ($n = 3$ independent experiments).

at CD30-encoding gene *Tnfrsf8* in both mouse CD4$^+$ and CD8$^+$ T-cells (Figure 2E). This result may reflect a previous ATAC-Seq (assay for transposase-accessible chromatin using sequencing) analysis showing that *Tnfrsf8* was one of the 263 genes marked by peaks after acetate treatment in CD8$^+$ T cells (Supplemental Figure S1G; Qiu *et al.*, 2019). We also performed ChIP (chromatin immunoprecipitation)-qPCR and found that supplemental acetate promotes H3K27ac at the locus of *Tnfrsf8* in mouse T cells (Figure 2, F and G; Qiu *et al.*, 2019).

Next, we focused on whether this transcriptional regulation of *Tnfrsf8* by acetate affects its protein expression. As expected, expression of CD30 protein was markedly increased by adding acetate in both mouse and human T-cells (Figure 2, H–J; Supplemental Figure S1, H–J). Because CD30 was identified as a cell surface protein (Stein *et al.*, 1982), we further conducted flow cytometry to detect cell surface expression of the CD30 protein. Similarly, acetate treatment resulted in enhanced expression of cell-surface CD30 protein (Figure 2, K–N; Supplemental Figure S1, K and L). Overall, our data suggest that acetate is a metabolic mediator of CD30 by positively regulating its expression through increasing gene-associated H3K27Ac levels.

CD30 modulates acetate-associated α-tubulin acetylation and microtubule stability

While supplementing the culture media with acetate can significantly increase CD30 levels, it is important to note that our RNA-Seq analysis reveals a potential role of CD30 in the positive regulation of cell apoptosis (Figure 1, I and J). We reasoned that if an increase in CD30 levels was critical, CD30 knockout might strengthen the ability of acetate to inhibit T-cell apoptosis by promoting acetate-associated α-tubulin acetylation and microtubule stability. Consistent with this notion, we utilized previously described CD30 knockout (*Cd30*$^{-/-}$) mice (Amakawa *et al.*, 1996) and showed that genetic disruption of *CD30* augmented the magnitude of acetate-mediated α-tubulin acetylation (Figure 3A; Supplemental Figure S2A), implicating CD30 in regulating α-tubulin acetylation. Moreover, α-tubulin acetylation has been shown to contribute to α-tubulin polymerization, leading to stabilization of microtubules (Yun *et al.*, 2021; Lyu *et al.*, 2022). The microtubules of Cd30-knockout T-cells were markedly more polymerized after treatment with acetate, which is consistent with a role for CD30 in suppressing α-tubulin acetylation (Figure 3, B–E).

Next, we sought to determine how CD30 deficiency could potentiate acetylation of α-tubulin and thereby modulate acetate-mediated microtube stability. Previous observations found that HDAC6 is a microtubule-associated deacetylase (Hubbert *et al.*, 2002) and that the cell–surface membrane glycoprotein CD133 is physically associated with HDAC6 in the cytoplasm and regulates its deacetylase activity (Mak *et al.*, 2012). We therefore reasoned that CD30 might interact with and stabilize HDAC6, maintaining its enzymatic activity to favor deacetylation of α-tubulin. We used a coimmunoprecipitation (co-IP) approach and found that HDAC6 pulled down CD30 (Figure 3F). Similar results were obtained using antibodies against CD30 for co-IP assays (Supplemental Figure S2B). To confirm these results and visualize where CD30 associates with HDAC6, we performed immunofluorescence analysis. Consistent with our co-IP results, CD30 colocalized with the cytoplasmic HDAC6 in WT T-cells, while only HDAC6 staining was observed in *Cd30*$^{-/-}$ T cells (Figure 3, G and H; Supplemental Figure S2, C and D).

We then assessed whether knockout of CD30 affects HDAC6 stability by treating T-cells with the protein synthesis inhibitor cycloheximide. HDAC6 exhibited a shorter half-life in *Cd30*$^{-/-}$ T-cells, compared with WT controls (Figure 3, I and J; Supplemental Figure S2, E and F), consistent with a role for CD30 in stabilizing HDAC6 protein. Additionally, *Cd30*$^{-/-}$ T-cells had reduced enzyme activity of HDAC6 (Figure 3K; Supplemental Figure S2G) and the HDAC6-selective inhibitor tubacin suppressed CD30-dependent deacetylation of α-tubulin (Figure 3L). Together, these results suggest that CD30 restrains the magnitude of acetate-mediated α-tubulin acetylation by interacting with and stabilizing HDAC6. In addition, acetate-treated T-cells considerably increased in cellular granularity without affecting overall cell size (Supplemental Figure S2, H–J). Cellular granularity has been shown to relate to proteomic abundance (Adrover *et al.*, 2020). While acetate supplementation increased the levels of CD30 protein, which in turn stabilized HDAC6, our data suggest that the combined action of increased acetate and reduced CD30 levels might help identify additional protein targets in this regulatory pathway.

Acetate coordinates with CD30 to modulate T-cell survival via a microtubule-Bcl-2 signaling axis

To better understand how CD30 might regulate acetate-mediated T-cell apoptosis, we performed a proteomics profile using mouse CD4$^+$ WT and *Cd30*$^{-/-}$ T-cells after treatment with acetate (Figure 4, A–C and Supplemental Table S2). Surprisingly, the bubble plot for KEGG (*Kyoto Encyclopedia of Genes and Genomes*) pathway analysis demonstrated that the "apoptosis" category was most significantly enriched for the differentially expressed protein-coding genes between *Cd30*$^{-/-}$ T-cells and their WT controls (Figure 4A). In addition to this result, our GO analysis pinpointed cell death as a significant molecular function pathway (Supplemental Figure S2K).

To further dissect the mechanism underlying the role of CD30 in T-cell acetate signaling, we performed heat map plot analysis for all the protein-coding genes within this apoptosis pathway category using our proteomic data (Figure 4B). Impressively, CD30 knockout T-cells showed an up-regulation of proteins encoded by all the anti-apoptotic genes (*Actg1*, *Bcl2*, *Bcl2l1* and *Mcl1*) (Cory and Adams, 2002; Zhou *et al.*, 2020), as well as a simultaneous decrease in the levels of all the pro-apoptotic proteins (cathepsin B encoded by *Ctsb*, cytochrome C encoded by *Cycs*, phosphoinositide-3-kinase regulatory subunit 2 encoded by *Pik3r2* and *Tradd*; Jiang and Wang, 2004; Gao *et al.*, 2016; Xu *et al.*, 2020; Chen *et al.*, 2021; Figure 4B). Among the 222 up-regulated proteins, anti-apoptotic Bcl-2 family proteins (Bcl-2 encoded by *Bcl2*, Bcl-xL encoded by *Bcl2l1*, and Mcl-1 encoded by *Mcl1*) appeared to play key roles in the regulation of apoptosis by acetate and CD30 (Figure 4C; Supplemental Figure S2L). Furthermore, gene set enrichment analysis (GSEA) showed enrichment of gene signature related to Bcl-2 signaling (Supplemental Figure S2M).

(F) Integrative Genomics Viewer displays ChIP-Seq analysis of H3K27ac at the locus of *Tnfrsf8* in mouse CD8$^+$ T-cells with or without acetate treatment. (G) ChIP–qPCR analysis of H3K27ac at the locus of *Tnfrsf8* in mouse T-cells with acetate treatment (n = 3 independent experiments). (H–J) Western blot of CD30 protein expression in mouse CD4$^+$, H, or CD8$^+$, I, T-cells and human T-cells, J, with or without acetate treatment (n = 3 independent experiments). (K–N) Flow cytometric analysis and median fluorescence intensity (MFI) quantification of CD30 protein levels in mouse CD4$^+$, K and L, or CD8$^+$, M and N, T-cells with or without acetate treatment (n = 3 independent experiments).

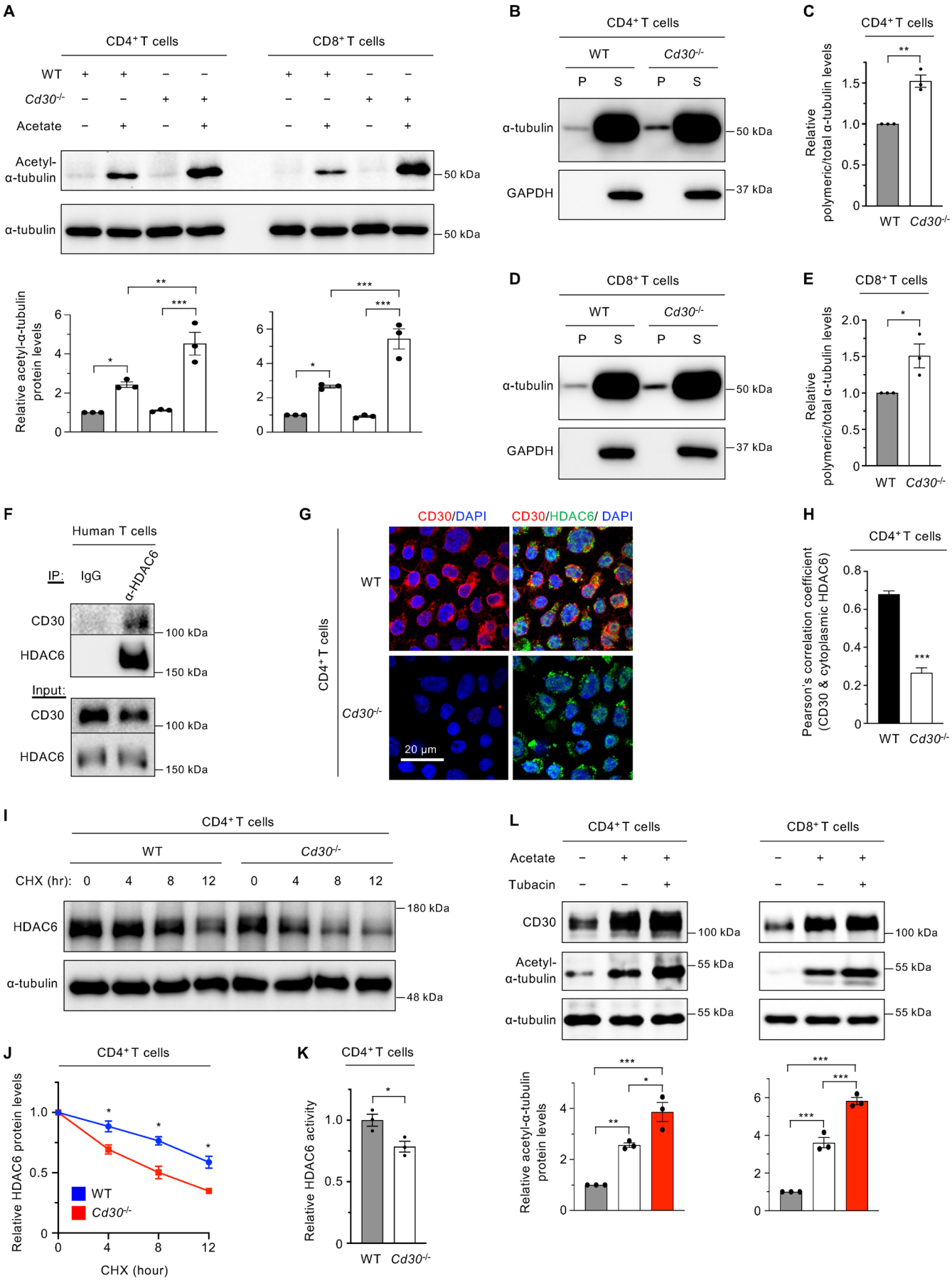
A
CD4+ T cells
CD8+ T cells
WT
Cd30-/-
Acetate
Acetyl-α-tubulin
α-tubulin
50 kDa
Relative acetyl-α-tubulin protein levels
B
CD4+ T cells
WT
Cd30-/-
P
S
α-tubulin
GAPDH
50 kDa
37 kDa
C
CD4+ T cells
Relative polymeric/total α-tubulin levels
D
CD8+ T cells
E
CD8+ T cells
F
Human T cells
IP:
IgG
α-HDAC6
CD30
HDAC6
Input:
100 kDa
150 kDa
G
CD30/DAPI
CD30/HDAC6/ DAPI
CD4+ T cells
20 μm
H
CD4+ T cells
Pearson's correlation coefficient (CD30 & cytoplasmic HDAC6)
I
CD4+ T cells
CHX (hr): 0 4 8 12 0 4 8 12
HDAC6
180 kDa
48 kDa
J
CD4+ T cells
Relative HDAC6 protein levels
CHX (hour)
K
CD4+ T cells
Relative HDAC6 activity
L
CD4+ T cells
CD8+ T cells
Tubacin
CD30
Acetyl-α-tubulin
55 kDa

To validate our proteomics analysis, we performed Western blotting and demonstrated that the anti-apoptotic Bcl-2 family members Bcl-2, Bcl-xL, and Mcl-1 were up-regulated by *Cd30* deletion and acetate (Figure 4, D–F; Supplemental Figure S2, N–Q). Furthermore, this increase in anti-apoptotic Bcl-2 family protein levels could inhibit doxorubicin-induced T-cell apoptosis, as evidenced by a marked reduction in caspase-3 signaling (Figure 4G). Based on these results, we propose a model in which acetate signaling results in a negative feedback loop catalyzed by an increase in CD30 expression, a subsequent stabilization of the deacetylase HDAC6, and a restraining effect on α-tubulin acetylation. This regulatory loop between acetate and CD30 orchestrates microtubule stability and the anti-apoptotic Bcl-2 signaling pathway (Figure 4H).

Our data suggest that increasing acetate levels protect T-cells from apoptosis, broadly consistent with an emerging role for acetate in protection from enteropathogenic infection (Fukuda *et al.*, 2011). In addition, we found that CD30 had an opposing effect on T cell apoptosis. Fortunately, many pharmacological approaches to target CD30 already exist, including the use of humanized monoclonal antibodies against CD30 (Croft *et al.*, 2013; van der Weyden *et al.*, 2017). Although our data linked acetate to T-cell apoptosis through the regulation of CD30 expression and α-tubulin acetylation, we cannot exclude the possibility that acetate treatment and hence increasing acetyl-CoA levels might have additional epigenetic effects on T-cell survival (e.g., through RNA acetylation or H3K27ac-mediated transcriptional regulation of other genes such as *Il2ra*; Li *et al.*, 2017; Narita *et al.*, 2019). Moreover, our results suggested that CD30 might potentially have effects on apoptosis that are independent of acetylated α-tubulin (Supplemental Figure S2N). Finally, our proteomic profiling of *Cd30*$^{-/-}$ T-cells also identified a panel of down-regulated proapoptotic proteins (e.g., Ctsb, Cycs, Pik3r2, and Tradd) that may merit further evaluation (Figure 4B). In summary, we demonstrate that the short-chain fatty acid acetate works together with CD30 to modulate T-cell apoptosis. Moreover, this study establishes a negative-feedback regulatory loop formed by acetate and CD30 for modulation of a microtubule-Bcl-2 anti-apoptotic signaling axis.

MATERIALS AND METHODS

Mice

Cd30 heterozygous mice (Amakawa *et al.*, 1996) were obtained from the Jackson Laboratory through cryorecovery (Stock No. 004457; The Jackson Laboratory) to generate *Cd30* knockout (*Cd30*$^{-/-}$) mice by heterozygous crossing. Unless stated otherwise, both female and male mice from six to twelve weeks old were used in the experiments. All mice were on a C57BL/6J (Stock No. 000664; The Jackson Laboratory) background, genotyped by standard PCR-based methods according to the Jackson Laboratory's protocol, and housed in a pathogen-free animal facility at the Johns Hopkins University School of Medicine. All the procedures were performed following the guidelines of the Institutional Animal Care and Use Committee.

Cells

Mouse CD4$^+$ or CD8$^+$ T-cells were isolated from the lymph nodes and spleen of *Cd30*$^{-/-}$ mice and control mice using the EasySep Mouse CD4$^+$ T cell Isolation Kit or EasySep Mouse CD8$^+$ T cell Isolation Kit. T cells were activated using Armenian hamster monoclonal anti-mouse CD3 (2 μg/ml; 100339, BioLegend; clone: 145-2C11; verified application includes cell activation) and Syrian hamster monoclonal anti-mouse CD28 (1 μg/ml; 102116, BioLegend; clone: 37.51; verified application includes cell activation) antibodies for three days. The ACK lysis buffer (A1049201, Thermo Fisher Scientific) was used to lyse the red blood cells. T-cells were cultured in RPMI 1640 (R8758, Sigma-Aldrich) supplemented with 10% (vol/vol) heat-inactivated fetal bovine serum (FBS; HyClone), glutamine (4 mM), penicillin/streptomycin (1%), and 2-mercaptoethanol (55 μM). After three days, these cells were cultured in RPMI 1640 supplemented with 10% heat-inactivated FBS, glutamine (4 mM), penicillin/streptomycin (1%), 2-mercaptoethanol (55 μM), and rhIL-2 (100 U/mL). Human peripheral blood mononuclear cells (PBMCs) were isolated from 20 ml of healthy donors' whole blood diluted with phosphate-buffered saline (PBS; 21-040-CM, Corning) at a ratio of 1:1 using Corning lymphocyte separation medium–gradient separation (25-072-CV, Corning). The ACK lysis buffer was used to lyse the red blood cells. PBMCs were activated using CD3/CD28 beads (11131D, Thermo Fisher Scientific) for three days. Activated PBMCs were cultured in RPMI 1640 supplemented with 10% heat-inactivated FBS, glutamine (4 mM), penicillin/streptomycin (1%), and rhIL-2 (100 U/ml). T-cells were isolated from the expanded PBMCs using a MojoSort Isolation Kit (480021, BioLegend). Human 293T cells (ATCC) were cultured in DMEM (D5796, Sigma-Aldrich) supplemented with 10% FBS, 100 U/ml penicillin, and 100 μg/ml streptomycin. All cells were cultured in a 37°C, 5% CO_2 tissue-culture incubator.

Chemicals, plasmids, and lentiviral vectors

T-cells were seeded in 24-well or 6-well plates and treated or not treated with 10 mM acetate (S5636, Sigma-Aldrich) for indicated times. Mouse T-cells were treated with doxorubicin (D1515, Sigma-Aldrich) at a final concentration of 5 μM for 8 h or 24 h. Mouse T-cells were treated or not treated with 20 μg/ml cycloheximide (C7698, Sigma-Aldrich) under 10 mM acetate for 0, 4, 8, and 12 h, respectively. The HDAC6-selective inhibitor tubacin (13691, Cayman Chemical) was used at a final concentration of 1 μM. Acetate and doxorubicin were used in 293T cells at final concentrations of 20 mM and 10 μM, respectively. WT α-tubulin (Tubulin-WT) plasmid

FIGURE 3: CD30 negatively regulates α-tubulin acetylation and microtubule stability. (A) Western blot of α-tubulin acetylation in WT control or *Cd30*$^{-/-}$ T-cells, with or without acetate treatment ($n = 3$ independent experiments). (B, C) Representative Western blot, B, and quantification, C, of microtubule polymerization in WT control or *Cd30*$^{-/-}$ CD4$^+$ T-cells treated with acetate ($n = 3$ independent experiments). (D, E) Representative Western blot, D, and quantification, E, of microtubule polymerization in WT or *Cd30*$^{-/-}$ CD8$^+$ T-cells treated with acetate ($n = 3$ independent experiments). (F) HDAC6 coimmunoprecipitates with CD30. Data represent one of two independent experiments. (G, H) Representative immunostaining images, G, and quantification, H, of colocalization between CD30 and HDAC6 in WT or *Cd30*$^{-/-}$ CD4$^+$ T-cells treated with acetate ($n = 10$ cells). (I, J) Representative Western blot, I, and quantification, J, of endogenous HDAC6 in WT or *Cd30*$^{-/-}$ CD4$^+$ T-cells treated with acetate and cycloheximide (CHX) ($n = 3$ independent experiments). (K) HDAC6 activity analysis of WT or *Cd30*$^{-/-}$ CD4$^+$ T-cells treated with acetate ($n = 3$ independent experiments). (L) Western blot of α-tubulin acetylation in mouse T-cells with or without acetate treatment, and with or without tubacin treatment ($n = 3$ independent experiments).

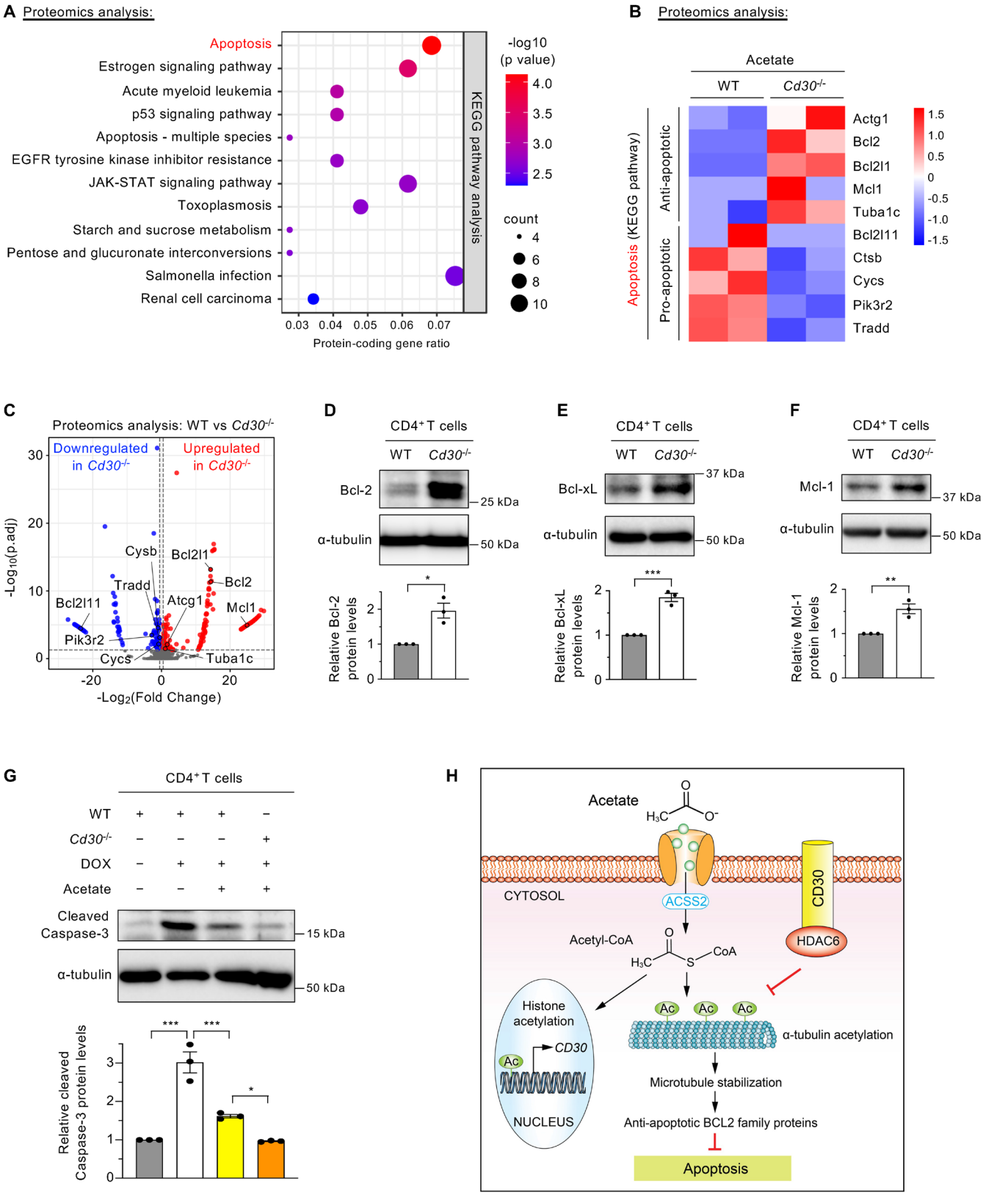

FIGURE 4: Acetate and CD30 collaboratively modulate T-cell apoptosis via a microtubule-Bcl-2 axis. (A) Bubble plot depicting top KEGG pathways for the differentially expressed protein-coding genes from proteomics data of WT or *Cd30*$^{-/-}$ CD4^{+} T-cells treated with acetate ($n = 2$ biological replicates). (B) Heat map analysis of the differentially expressed proteins in the KEGG category "Apoptosis" from proteomics data of WT or *Cd30*$^{-/-}$ CD4^{+} T-cells treated with acetate ($n = 2$ biological replicates). (C) Volcano plot of significantly differentially expressed proteins in acetate-treated *Cd30*$^{-/-}$ CD4^{+} T-cells, compared with WT. The -$\log_{10}$ (adjusted p value) was plotted against the $\log_2$(Fold Change) in

and its mutant version with K40R (Tubulin-K40R) were used (Gao *et al.*, 2010). pMD2.G (12259, Addgene), psPAX2 (12260, Addgene), and pCDH-EF1-FHC (64874, Addgene) were from Addgene. Flag-tagged Tubulin-WT and Tubulin K40R plasmids were amplified by PCR with Q5 high-fidelity DNA polymerase (M0491S, New England Baobabs) and deoxynucleotide (dNTP) solution mix (N0447S, New England Baobabs) using EGFP-Tubulin WT and EGFP-Tubulin K40R as templates (Gao *et al.*, 2010). Full sequence information on the templates was obtained from Addgene (Plasmids #30487 and #30488) and our colonies were verified by DNA sequencing (Eurofins Genomics). For tubulin cloning, the following primers were used: forward primer, 5′- CTAGCTAGCATGCGTGAGTGCATCTCCAT-3′, and reverse primer, 5′- CGCGGATCCGTATTCCTCTCCTTCTTCCT-3′. PCR product was purified using DNA Clean & Concentrator-5 (D4003, ZYMO RESEARCH) and then cloned in pCDH-EF1-FHC vector backbone. pCDH-EF1-FHC vector (64874, Addgene) was transformed in Stbl3 E. coli cells (C737303, Thermo Fisher Scientific), amplified in bacteria, and then extracted with the ZymoPURE Plasmid Miniprep Kit (D4212, ZYMO RESEARCH). The purified PCR product and vector were digested by *Nhe*I (R3131S, New England Biolabs) and *Bma*HI (R3136S, New England Biolabs) restriction enzymes. The purified digestion product was ligated by T4 DNA Ligase (M0202S, New England Biolabs). Stbl3 *E. coli* cells was transformed by heat shock with a ligation reaction and plated onto an LB medium containing ampicillin (A1593, Sigma-Aldrich). Flag-Tubulin-WT and Flag-Tubulin-K40R were amplified in bacteria and extracted with a ZymoPURE Plasmid Miniprep Kit. The pMD2.G (12259, Addgene) and the psPAX2 (12260, Addgene) were amplified in bacteria and extracted with a ZymoPURE Plasmid Miniprep Kit. Human 293T cells were transfected by Flag-Tubulin-WT or Flag-Tubulin-K40R together with package vectors (pMD2.G and psPAX2) using PEI (919012, Sigma-Aldrich) for two days. Lentiviral supernatants were collected and stored at –80°C. Cells were incubated overnight with the virus mixture in the presence of polybrene (sc-134220, Santa Cruz Biotechnology) at a final concentration of 5 μg/ml and then subjected to two-day selection with puromycin (P8833, Sigma-Aldrich; 1 μg/ml).

Real-time quantitative reverse transcription PCR

Activated mouse $CD4^+$ T-cells, activated mouse $CD8^+$ T-cells, and activated human T-cells were seeded in 24-well plates and treated or not treated with 10 mM sodium acetate for one day. Total RNA was extracted using Direct-zol RNA Miniprep Plus (R2072, ZYMO RESEARCH), during which DNase digestion was performed using DNase I. cDNA was synthesized with an iScript cDNA Synthesis Kit (1708891, Bio-Rad Laboratories). The *CD30* mRNA expression was detected on a CFX Connect Real-Time System (Bio-Rad Laboratories) using THUNDERBIRD SYBR qPCR mix (QPS-201, Toyobo). Bio-Rad CFX Maestro software was used to acquire data. Either human *RPL7* or mouse *Rpl7* was used as the internal control. Relative mRNA level was quantitated using the comparative CT ($2^{-\Delta\Delta Ct}$) method. The primers were synthesized by Integrated DNA Technologies (Coralville, IA). The following primers were used to detect gene expression: human *CD30*, forward primer, 5′-AATTCGGCAGAAGCTCCACC-3′, and reverse primer, 5′-TTGAGCTCCTCCTGGGTCTG-3′; human *RPL7*, forward primer, 5′-CAAGGCTTCGATTAACATGCTGA-3′, and reverse primer, 5′-GCCATAACCACGCTTGTAGATT-3′; mouse *Cd30*, forward primer, 5′-CCTTCCCAACGGATCGACC-3′, and reverse primer, 5′-CCCGTCTTCATTGACGTAGTAGT-3′; mouse *Rpl7*, forward primer, 5′-AGCACTATCACAAGGAGTACAGG-3′, and reverse primer, 5′-GCACATAGAAGTTGCCAGCTT-3′.

Immunofluorescence

For acetylated α-tubulin staining, T-cells were seeded in 24-well plates and treated or not treated with 10 mM sodium acetate for one day. For CD30 and HDAC6 staining, cells were seeded in 24-well plates and treated or not treated with 10 mM sodium acetate for three days. After treatment, 1×10^5 of each cell suspension was plated onto a cell culture–treated 15-well μ-Slide Angiogenesis ibiTreat chamber slide (81506, Ibidi) or added to a slide chamber and then spun down onto the slide using a Cytospin 4 centrifuge (800 rpm for 3 min, Thermo Fisher Scientific). Cells were fixed at room temperature with 4% paraformaldehyde (28908, Thermo Fisher Scientific) for 20 min and then permeabilized at room temperature with 0.5% Triton X-100 (1610407, Bio-Rad Laboratories) for 15 min. Cells were blocked with 3% bovine serum albumin (10735108001, Sigma-Aldrich) in PBS (21-040-CM, Corning) containing 0.05% Tween-20 for 1 h. Then the cells were incubated overnight at 4°C with the following validated antibodies for immunofluorescence (species reactivity includes mouse): rabbit monoclonal anti-CD30 (54535S, Cell Signaling Technology), mouse monoclonal anti-HDAC6 (GTX84377, GeneTex) primary antibodies, or mouse monoclonal anti-acetylated-α-tubulin Alexa Fluor 488 primary antibody (sc-23950, Santa Cruz Biotechnology). For acetylated-α-tubulin staining, average fluorescence intensity (AFI) was determined by dividing the overall mean florescence intensity by the area of the cell from at least 10 cells and quantified using ImageJ. For CD30 and HDAC6 staining, the cells were incubated with donkey anti-mouse secondary antibodies conjugated to Alexa Fluor488 (A-21202, Thermo Fisher Scientific) or goat anti-rabbit secondary antibodies conjugated to Alexa Fluor568 (A-11036, Thermo Fisher Scientific) for 1 h at room temperature. The nuclei were stained with DAPI (62248, Thermo Fisher Scientific) for 5 min at room temperature. The cells were mounted with Immu-mount (9990402, Epredia) and observed under a Nikon Eclipse Ti2 confocal microscope. Images were acquired using NIS-Elements Imaging Software (version 5.21.03). For colocalization assessment, the intensity correlation analysis was calculated from at least 10 cells and quantified using ImageJ as previously described (Xiong *et al.*, 2015).

gene expression. Up-regulated proteins in $Cd30^{-/-}$ $CD4^+$ T-cells ($n = 222$; $\log_2$[Fold Change] > 0.5; adjusted p value < 0.05)] are depicted as red dots; genes that were down-regulated in $Cd30^{-/-}$ $CD4^+$ T-cells ($n = 151$; $\log_2$[Fold Change] < –0.5; adjusted p value < 0.05) are depicted in blue ($n = 2$ biological replicates). (D–F) Western blot of Bcl-2, D,, Bcl-xL, E, and Mcl-1, F, in T-cells with acetate treatment ($n = 3$ independent experiments). (G) Western blot of cleaved caspase-3 in the context of DOX-induced T-cell apoptosis ($n = 3$ independent experiments). (H) A model for how acetate works together with CD30 to modulate T-cell survival. In the setting of T-cell apoptosis, acetate treatment causes an increase in acetyl CoA levels, resulting in acetylation of α-tubulin, as well as transcriptional activation of *Tnfrsf8*. CD30 in turn negatively regulates α-tubulin acetylation through stabilization of the deacetylase HDAC6. This cooperation between acetate and CD30 mediates microtubule stability and the anti-apoptotic Bcl-2 signaling pathway.

Western blot analysis

For Cleaved Caspase-3 detection, mouse T-cells were seeded in 24-well plates and treated or not treated with 10 mM sodium acetate (S5636, Sigma-Aldrich) for 16 h. The cells were then treated or not treated with 5 μM doxorubicin (D1515, Sigma-Aldrich) for another 8 h. For acetyl Histone H3 detection, mouse T-cells were seeded in 24-well plates and treated or not treated with 10 mM sodium acetate for 24 h. For CD30 detection, mouse T-cells and human T-cells were seeded in 24-well plates and treated or not treated with 10 mM sodium acetate for two days. For acetyl-α-tubulin detection, mouse T-cells were seeded in 24-well plates and treated or not treated with 10 mM sodium acetate for 4 h. For Bcl-2 family protein detection, mouse T-cells were seeded in 24-well plates and treated or not treated with 10 mM sodium acetate for 24 h. For human 293T cells apoptosis detection, cells were seeded in 6-well plates at a density of 6×10^5 per well. Finally, the cells were lysed using RIPA buffer (BP-115, Boston BioProducts) containing protease inhibitor (11836170001, Roche Life Sciences) and phosphatase inhibitor cocktails (04906837001, Roche Life Sciences). Protein concentration was measured using a Pierce BCA Protein Assay Kit (23225, Thermo Fisher Scientific). The protein lysates were heated at 95°C with 4 × Laemmli sample buffer (1610747, Bio-Rad Laboratories) for 10 min and then separated on a 10% or 15% SDS–PAGE gel. The separated proteins were transferred onto the nitrocellulose membranes and the membranes were blocked with 5% nonfat dry milk for 1 h at room temperature. The membranes were incubated with the indicated primary antibodies overnight at 4°C, followed by horseradish peroxidase (HRP)–conjugated secondary antibodies for 1 h at room temperature.

The following validated antibodies for Western blotting (species reactivity includes human and mouse) were used. Primary antibodies against α-tubulin (mouse monoclonal; T5168) and FLAG (rabbit polyclonal; F7425) were purchased from Sigma-Aldrich. Rabbit monoclonal primary antibodies against acetyl-α-tubulin (5335S), CD30 (54535S), Histone H3 (4499S), acetyl Histone H3 (Lys27) (8173S), and Cleaved Caspase-3 (9664S) were purchased from Cell Signaling Technology. Mouse monoclonal primary antibodies against Bcl-xL (sc-8392) and Mcl-1 (sc-74437) were purchased from Santa Cruz Biotechnology. Rabbit polyclonal primary antibody against Bcl-2 (ab196495) was purchased from Abcam. HRP-linked secondary antibodies, goat anti-mouse IgG (H + L)–HRP conjugate (170-6516), and goat anti-rabbit IgG (H + L)–HRP conjugate (170-6515) were purchased from Bio-Rad Laboratories. The protein bands were detected with Clarity Western ECL Substrate (1705061, Bio-Rad Laboratories) under a ChemiDoc MP imaging system (Bio-Rad Laboratories). Image Lab was used to acquire and analyze Western blot images.

Coimmunoprecipitation analysis

Human T-cells were cultured as described above. A sample of 2.5×10^7 of the cells was treated or not treated with 10 mM sodium acetate for two days. The cells were washed with cold PBS, pelleted by centrifugation, and resuspended in an IP lysis buffer (87788, Thermo Fisher Scientific) containing protease inhibitor and phosphatase inhibitor cocktails. The total protein was incubated overnight at 4°C with the following validated antibodies for IP (species reactivity includes human): mouse monoclonal anti-HDAC6 (sc-28386, Santa Cruz Biotechnology), IgG (61656S, Cell Signaling Technology), rabbit polyclonal anti-CD30 (PA5-86095, Thermo Fisher Scientific) or IgG (3900S, Cell Signaling Technology) antibodies, and Protein A (10006D, Thermo Fisher Scientific) or Protein G (10007D, Thermo Fisher Scientific) Beads. After being washed with 1 × Wash Buffer, the beads were collected by centrifugation and resuspended in SDS loading buffer. Immunoprecipitated proteins were separated by 10% SDS–polyacrylamide gel electrophoresis (SDS–PAGE). Western blot assays for CD30 (54535S, Cell Signaling Technology; validated rabbit monoclonal antibody for use in Western blotting detection of endogenous CD30; species reactivity includes human) and HDAC6 (7612S, Cell Signaling Technology; validated rabbit monoclonal antibody for use in Western blotting detection of endogenous HDAC6; species reactivity includes human) were performed as described above.

Acetyl CoA assay

Mouse and human T-cells were cultured as described above. The cells were treated or not treated with 10 mM sodium acetate for one day. The cell pellet was lysed using Dounce homogenizer. The intracellular acetyl CoA levels were determined by an Acetyl CoA Assay Kit (ab87546, Abcam) following the manufacturer's manual. The deproteinization step requires 4 M perchloric acid (PCA) and 2 M potassium hydroxide (KOH). Briefly, for the acetyl CoA measurement, free CoA is quenched and then acetyl CoA is enzymatically converted to CoA at 37°C for 10 min. The CoA was reacted with a specific probe to form NADH, generating fluorescence (Ex/Em = 535/587), and the fluorometric readout was monitored using a multimode plate reader (Perkin Elmer).

HDAC6 activity measurement

Mouse T-cells were cultured as described above and then were treated or not treated with 10 mM sodium acetate for 4 h. The cell pellet was lysed using Dounce homogenizer. The intracellular HDAC6 activity was detected using an HDAC6 Activity Assay Kit (ab284549, Abcam) following the manufacturer's manual. Briefly, HDAC6 activity measurement utilizes deacetylase activity of HDAC6 toward a synthetic acetylated-peptide substrate, resulting in the release of an AFC fluorophore (Ex/Em 380/490 nm). The fluorometric readout was monitored using a multimode plate reader (Perkin Elmer).

HDAC6 stability assay

Mouse $CD4^+$ T-cells and mouse $CD8^+$ T-cells were cultured as described above. Cells were treated or not treated with 20 μg/ml cycloheximide (C7698, Sigma-Aldrich) under 10 mM sodium acetate for 0, 4, 8, or 12 h. Western blot assays for HDAC6 (7612S, Cell Signaling Technology; validated rabbit monoclonal antibody for use in Western blotting detection of endogenous HDAC6; species reactivity includes mouse) and α-tubulin (T5168, Sigma-Aldrich; validated mouse monoclonal antibody for use in Western blotting detection of endogenous α-tubulin; species reactivity includes mouse) were performed as described above.

Microtubule stability assay

A microtubule stability assay was conducted as reported previously (Nishida *et al.*, 2005). Mouse T-cells were cultured as described above and then treated with 10 mM sodium acetate for two days. A sample of 1×10^6 of the cells were suspended in 200 μl of extraction buffer, containing 0.1 M PIPES, pH 7.1, 1 mM $MgSO_4$, 1 mM EGTA, 2 M glycerol, and 0.1% Triton X-100, as well as a protease inhibitor and a phosphatase inhibitor cocktail. After incubation on ice for 15 min, the cell lysates were centrifuged at 15,000 rpm for 15 min at 4°C, and then the supernatant that contained soluble tubulin was collected. The remaining pellet was resuspended in lysis buffer that contained 25 mM Tris-HCl, pH 7.4, 0.4 M NaCl, and 0.5% SDS. and boiled for 10 min. The sample was centrifuged at 15,000 rpm for 5 min at room temperature. The supernatant that contained polymeric tubulin was collected. The soluble (S) and polymerized (P)

tubulin were subjected to SDS–PAGE and detected by Western blot using mouse monoclonal anti-α-tubulin antibody (T5168, Sigma-Aldrich; validated mouse monoclonal antibody for use in Western blotting detection of endogenous α-tubulin; species reactivity includes mouse). A rabbit monoclonal anti-GAPDH antibody (5174S, Cell Signaling Technology; validated rabbit monoclonal antibody for use in Western blotting detection of endogenous GAPDH; species reactivity includes mouse) was used as a loading control for each experiment. The microtubule polymerization was quantitated based on the relative amount of polymerized (P) out of total (P+S) using Image Lab.

Flow cytometry analysis

Mouse and human T-cells were cultured as described above. For the cell apoptosis assay, mouse $CD4^+$ T-cells and mouse $CD8^+$ T-cells were treated or not treated with 10 mM acetate for 24 h and then the cell cultures 5 μM doxorubicin and 10 mM acetate were added or not added for another 24 h. The percentage of annexin V^+ apoptotic cells was detected using an FITC Annexin V apoptosis detection kit with PI (PI, propidium iodide; 640914, BioLegend), based on the manufacturer's instructions. For cell surface staining, mouse $CD4^+$ T-cells, mouse $CD8^+$ T-cells, and human T-cells were treated or not treated with 10 mM acetate for two days. Surface staining was performed for 20 min in PBS containing 2% FBS at 4°C. The following validated antibodies for flow cytometry were used for cell staining: PE anti-human CD30 antibody (mouse monoclonal; 333906, BioLegend), FITC anti-human CD3 antibody (mouse monoclonal; 300306, BioLegend), PE anti-mouse CD30 antibody (Armenian hamster monoclonal; 102306, BioLegend), FITC anti-mouse CD4 antibody (rat monoclonal; 100406, BioLegend), and FITC anti-mouse CD8a antibody (rat monoclonal; 100706, BioLegend). Data were acquired using a CytoFLEX flow cytometer (Beckman Coulter, Brea) and analyzed using FlowJo (v10.8.1, BD Biosciences).

Chromatin immunoprecipitation–quantitative polymerase chain reaction assay

Chromatin immunoprecipitation (ChIP) was performed using an EpiQuik chromatin immunoprecipitation (ChIP) kit (P-2002-3, EpiQuik) following the manufacturer's instructions. Cells were cross-linked in 1% formaldehyde and neutralized using 0.125 M glycine. The chromatin complex was sonicated using a Bioruptor sonication system (Diagenode, Denville, NJ). The sheared chromatin was immunoprecipitated with rabbit monoclonal anti-acetyl-histone H3 (Lys27) (8173S, Cell Signaling Technology) ChIP-grade antibodies using the protein A-precoated assay wells. The normal rabbit IgG (3900S, Cell Signaling Technology) was used as a nonspecific antibody control for immunoprecipitation. Protein–DNA cross-linking was reversed at 65°C. DNA was purified and analyzed by real-time qPCR assay. Enrichment of DNA was shown as the percentage (%) input according to the manufacturer's instructions. The calculation of the % input for each ChIP fraction is 2(–ΔCt [normalized ChIP]), where ΔCt [normalized ChIP] = (Ct [ChIP] - (Ct [Input] - Log2 (Input Dilution Factor))). Primers used in ChIP–qPCR analysis: forward, 5′-TGAATGAGAGCAAAGGTGGG-3′; reverse, 5′-CTATAGAACCAGAGACAGCACTG-3′.

Chromatin accessibility assay

CD30 gene promoter accessibility was determined using an EpiQuik chromatin accessibility assay kit (P-1047-48, Epigentek) following the protocol provided by the manufacturer. Chromatin was isolated from mouse $CD4^+$ or $CD8^+$ T-cells with or without acetate treatment. Then cells were treated with a nuclease (Nse) mix. DNA was then isolated and amplified using qPCR and gene-specific primers for CD30 (listed in ChIP–qPCR assay). The fold enrichment (FE) was calculated by the ratio of amplification efficiency of the Nse-treated DNA sample to that of a control sample that was not treated with a nuclease (no Nse). The fold change in enrichment was calculated using the formula FE = 2(NseCT- no NseCT) × 100%. FE% >1600% indicates that the gene region is in the opened chromatin, while FE% <400% represents that the gene region is in closed chromatin.

RNA-sequencing analysis

Total RNA was extracted from mouse $CD8^+$ T–cells with or without acetate treatment for 24 h using a Direct-zol RNA Miniprep Plus kit (R2073, Zymo Research, Irvine, CA). The sequencing libraries were constructed from 500 ng of total RNA using a Zymo-Seq RiboFree Total RNA Library Kit (R3000, Zymo Research, Irvine, CA) and the concentrations of RNA-Seq libraries were determined using a Qubit 4 instrument (Q33239, Thermo Fisher Scientific). RNA-Seq libraries were sequenced on an Illumina NovaSeq to a sequencing depth of at least 30 million read pairs (150 bp paired-end sequencing) per sample. The Zymo Research RNA-Seq pipeline was originally adapted from nf-core/rnaseq pipeline v1.4.2. The pipeline was built using Nextflow. Briefly, quality control of raw reads was carried out using FastQC v0.11.9. Adapter and low-quality sequences were trimmed from raw reads using Trim Galore! v0.6.6. Trimmed reads were aligned to the reference genome using STAR v2.6.1d. BAM file filtering and indexing were carried out using SAMtools v1.9. RNA-seq library quality control was implemented using RSeQC v4.0.0 and QualiMap v2.2.2-dev. Duplicate reads were marked using Picard tools v2.23.9. Library complexity was estimated using Preseq v2.0.3. Duplication rate quality control was performed using dupRadar v1.18.0. Reads overlapping with exons were assigned to genes using featureCounts v2.0.1. Classification of rRNA genes/exons and their reads were based on annotations and RepeatMasker rRNA tracks from a UCSC genome browser when applicable. Differential gene expression analysis was completed using DESeq2 v1.28.0. Functional enrichment analysis was achieved using g:Profiler python API v1.0.0 (https://biit.cs.ut.ee/gprofiler/gost). Quality control and analysis results plots were visualized using MultiQC v1.9. The RNA-Seq data were analyzed using an R programming environment and deposited in the Gene Expression Omnibus repository with accession number GSE217411.

Proteomics and mass spectrometry analysis

The sample preparation for mass spectrometry (MS)-based proteomics was performed on our previously published fully automated pipeline (Reilly *et al.*, 2021). Briefly, 2 million mouse $CD4^+$ T-cells of each replicate were washed three times with ice-cold PBS and lysed by 200 μl of high-percentage detergent SP3 lysis buffer (50 mM Tris-HCl (pH 8.0), 50 mM NaCl, 1% SDS, 1% triton X-100, 1% NP-40, 1% tween 20, 1% glycerol, 1% sodium deoxycholate [wt/vol], 5 mM EDTA [pH 8.0], 5 mM dithiothreitol, 5KU benzonase, and 1 × complete protease inhibitor). The cell lysate was heated to 65°C for 30 min and was alkylated for 30 min using iodoacetamide, followed by automated protein extraction and tryptic digestion overnight using a KingFisher APEX (Thermo Scientific) robot. The resulting peptides were measured and normalized using an automated colorimetric assay on a Bravo (Agilent Technologies) robot. The final resulting tryptic peptides were separated on a nano column (75 μm × 500 mm, 2 μm C_{18} particle) using a 2-h efficient linear gradient (Phase B, 2-35% ACN) on an UltiMate 3000 nano-HPLC system. We used data independent acquisition (DIA) discovery proteomics on a hybrid Orbitrap Eclipse mass spectrometer. Specifically, MS1 resolution was

set to 120K, and MS2 resolution was set to 30K. For DIA isolation, the precursor range was set to 400–1000 *m/z*, and the isolation window was 8 m/*z*, resulting in 75 windows for each scan cycle (3 s). High collision dissociation was used for fragmentation with 30% collision energy. The AGC target was set to 800% for MS2 scan (improve MS2 spectra quality). The MS2 scan range was defined as 145–1450 *m/z*, which covers the majority of fragment ions of typical tryptic peptides.

The database search was performed at the protein level by Spectronaut software 16.0. We used a library-free module (i.e., direct DIA), which does not require a preconstructed high-quality project-specific spectral library but only uses a proteome sequence file. Specifically, the MS/MS spectra were searched against a proteome reference database containing 17,125 proteins (reviewed) mapped to the mouse reference genome obtained via the UniProt Consortium. All spectra were allowed "trypsin and lysC" enzyme specificity, with up to two missed cleavages. Allowed fixed modifications included carbamidomethylation of cysteine and the allowed variable modifications for whole proteome datasets were acetylation of protein N-termini, oxidized methionine. The false discovery rates of peptide and protein were all set as 1%. Three replicate MS analyses were done from each sample. Further analysis was performed on the mean values of the replicate MS analyses. DESeq2 was implemented to analyze the differential expression between sample types. R software was used to analyze and visualize data ($n = 2$ biological replicates).

Statistics

The statistical significance of differences between control and test groups was determined by an unpaired two-tailed Student's *t* test unless mentioned otherwise. For Figures 1H, 3, A and L, and 4G and Supplemental Figure S1, A and C, the significance was determined via one-way ANOVA with Tukey's multiple comparison. Results are represented as the mean ± standard error of the mean (SEM) and *p* values < 0.05 were considered significant (*$p < 0.05$; **$p < 0.01$; ***$p < 0.001$; $n = 3$ independent experiments unless mentioned otherwise). GraphPad Prism 9 software (version 9.4.1; GraphPad Software, La Jolla, CA) was used for statistical calculations.

ACKNOWLEDGMENTS

We wish to acknowledge Timothy F. Osborne for critical reading of this manuscript, and members of the Leonard Lab for technical support. This work was supported by NIH Grant K22HL146793 to J.X.

REFERENCES

Adrover JM, Aroca-Crevillen A, Crainiciuc G, Ostos F, Rojas-Vega Y, Rubio-Ponce A, Cilloniz C, Bonzon-Kulichenko E, Calvo E, Rico D, *et al.* (2020). Programmed "disarming" of the neutrophil proteome reduces the magnitude of inflammation. Nat Immunol 21, 135–144.

Amakawa R, Hakem A, Kundig TM, Matsuyama T, Simard JJ, Timms E, Wakeham A, Mittruecker HW, Griesser H, Takimoto H, *et al.* (1996). Impaired negative selection of T cells in Hodgkin's disease antigen CD30-deficient mice. Cell 84, 551–562.

Balmer ML, Ma EH, Bantug GR, Grahlert J, Pfister S, Glatter T, Jauch A, Dimeloe S, Slack E, Dehio P, *et al.* (2016). Memory CD8(+) T cells require increased concentrations of acetate induced by stress for optimal function. Immunity 44, 1312–1324.

Bantug GR, Galluzzi L, Kroemer G, Hess C (2018). The spectrum of T cell metabolism in health and disease. Nat Rev Immunol 18, 19–34.

Cai L, Sutter BM, Li B, Tu BP (2011). Acetyl-CoA induces cell growth and proliferation by promoting the acetylation of histones at growth genes. Mol Cell 42, 426–437.

Chen C, Ahmad MJ, Ye T, Du C, Zhang X, Liang A, Yang L (2021). Cathepsin B regulates mice granulosa cells' apoptosis and proliferation *in vitro*. Int J Mol Sci 22.

Cory S, Adams JM (2002). The Bcl2 family: regulators of the cellular life-or-death switch. Nat Rev Cancer 2, 647–656.

Croft M, Benedict CA, Ware CF (2013). Clinical targeting of the TNF and TNFR superfamilies. Nat Rev Drug Discov 12, 147–168.

Fukuda S, Toh H, Hase K, Oshima K, Nakanishi Y, Yoshimura K, Tobe T, Clarke JM, Topping DL, Suzuki T, *et al.* (2011). Bifidobacteria can protect from enteropathogenic infection through production of acetate. Nature 469, 543–547.

Gamen S, Anel A, Lasierra P, Alava MA, Martinez-Lorenzo MJ, Pineiro A, Naval J (1997). Doxorubicin-induced apoptosis in human T-cell leukemia is mediated by caspase-3 activation in a Fas-independent way. FEBS Lett 417, 360–364.

Gao J, Zhou XL, Kong RN, Ji LM, He LL, Zhao DB (2016). MicroRNA-126 targeting PIK3R2 promotes rheumatoid arthritis synovial fibro-blasts proliferation and resistance to apoptosis by regulating PI3K/AKT pathway. Exp Mol Pathol 100, 192–198.

Gao YS, Hubbert CC, Yao TP (2010). The microtubule-associated histone deacetylase 6 (HDAC6) regulates epidermal growth factor receptor (EGFR) endocytic trafficking and degradation. J Biol Chem 285, 11219–11226.

Geltink RIK, Kyle RL, Pearce EL (2018). Unraveling the complex interplay between T cell metabolism and function. Annu Rev Immunol 36, 461–488.

Gu S, Liu Y, Zhu B, Ding K, Yao TP, Chen F, Zhan L, Xu P, Ehrlich M, Liang T, *et al.* (2016). Loss of alpha-tubulin acetylation is associated with TGF-beta-induced epithelial–mesenchymal transition. J Biol Chem 291, 5396–5405.

Hu M, Eviston D, Hsu P, Marino E, Chidgey A, Santner-Nanan B, Wong K, Richards JL, Yap YA, Collier F, *et al.* (2019). Decreased maternal serum acetate and impaired fetal thymic and regulatory T cell development in preeclampsia. Nat Commun 10, 3031.

Hubbert C, Guardiola A, Shao R, Kawaguchi Y, Ito A, Nixon A, Yoshida M, Wang XF, Yao TP (2002). HDAC6 is a microtubule-associated deacetylase. Nature 417, 455–458.

Jiang X, Wang X (2004). Cytochrome C-mediated apoptosis. Annu Rev Biochem 73, 87–106.

Jung J, Zeng H, Horng T (2019). Metabolism as a guiding force for immunity. Nat Cell Biol 21, 85–93.

Kendrick SF, O'Boyle G, Mann J, Zeybel M, Palmer J, Jones DE, Day CP (2010). Acetate, the key modulator of inflammatory responses in acute alcoholic hepatitis. Hepatology 51, 1988–1997.

Knipling L, Wolff J (2006). Direct interaction of Bcl-2 proteins with tubulin. Biochem Biophys Res Commun 341, 433–439.

Lee JV, Carrer A, Shah S, Snyder NW, Wei S, Venneti S, Worth AJ, Yuan ZF, Lim HW, Liu S, *et al.* (2014). Akt-dependent metabolic reprogramming regulates tumor cell histone acetylation. Cell Metab 20, 306–319.

Li P, Mitra S, Spolski R, Oh J, Liao W, Tang Z, Mo F, Li X, West EE, Gromer D, *et al.* (2017). STAT5-mediated chromatin interactions in superenhancers activate IL-2 highly inducible genes: functional dissection of the Il2ra gene locus. Proc Natl Acad Sci USA 114, 12111–12119.

Lyu J, Pirooznia M, Li Y, Xiong J (2022). The short-chain fatty acid acetate modulates epithelial-to-mesenchymal transition. Mol Biol Cell 33.

Mak AB, Nixon AM, Kittanakom S, Stewart JM, Chen GI, Curak J, Gingras AC, Mazitschek R, Neel BG, Stagljar I, Moffat J (2012). Regulation of CD133 by HDAC6 promotes beta-catenin signaling to suppress cancer cell differentiation. Cell Rep 2, 951–963.

Matharu N, Ahituv N (2020). Modulating gene regulation to treat genetic disorders. Nat Rev Drug Discov 19, 757–775.

Moffett JR, Puthillathu N, Vengilote R, Jaworski DM, Namboodiri AM (2020). Acetate revisited: a key biomolecule at the nexus of metabolism, epigenetics, and oncogenesis. Part 2: acetate and ACSS2 in health and disease. Front Physiol 11, 580171.

Mollinedo F, Gajate C (2003). Microtubules, microtubule-interfering agents and apoptosis. Apoptosis 8, 413–450.

Narita T, Weinert BT, Choudhary C (2019). Functions and mechanisms of non-histone protein acetylation. Nat Rev Mol Cell Biol 20, 156–174.

Nishida K, Yamasaki S, Ito Y, Kabu K, Hattori K, Tezuka T, Nishizumi H, Kitamura D, Goitsuka R, Geha RS, *et al.* (2005). FcepsilonRI-mediated mast cell degranulation requires calcium-independent microtubule-dependent translocation of granules to the plasma membrane. J Cell Biol 170, 115–126.

Peng M, Yin N, Chhangawala S, Xu K, Leslie CS, Li MO (2016). Aerobic glycolysis promotes T helper 1 cell differentiation through an epigenetic mechanism. Science 354, 481–484.

Pietrocola F, Galluzzi L, Bravo-San Pedro JM, Madeo F, Kroemer G (2015). Acetyl coenzyme A: a central metabolite and second messenger. Cell Metab 21, 805–821.
Qiu J, Villa M, Sanin DE, Buck MD, O'Sullivan D, Ching R, Matsushita M, Grzes KM, Winkler F, Chang CH, *et al*. (2019). Acetate promotes T cell effector function during glucose restriction. Cell Rep 27, 2063–2074 e2065.
Reilly L, Peng L, Lara E, Ramos D, Fernandopulle M, Pantazis CB, Stadler J, Santiana M, Dadu A, Iben J, *et al*. (2021). A fully automated FAIMS-DIA proteomic pipeline for high-throughput characterization of iPSC-derived neurons. https://doi.org/10.1101/2021.11.24.469921.
Schug ZT, Peck B, Jones DT, Zhang Q, Grosskurth S, Alam IS, Goodwin LM, Smethurst E, Mason S, Blyth K, *et al*. (2015). Acetyl-CoA synthetase 2 promotes acetate utilization and maintains cancer cell growth under metabolic stress. Cancer Cell 27, 57–71.
Stein H, Gerdes J, Schwab U, Lemke H, Mason DY, Ziegler A, Schienle W, Diehl V (1982). Identification of Hodgkin and Sternberg–Reed cells as a unique cell type derived from a newly-detected small-cell population. Int J Cancer 30, 445–459.
van der Weyden CA, Pileri SA, Feldman AL, Whisstock J, Prince HM (2017). Understanding CD30 biology and therapeutic targeting: a historical perspective providing insight into future directions. Blood Cancer J 7, e603.
Wong BW, Wang X, Zecchin A, Thienpont B, Cornelissen I, Kalucka J, Garcia-Caballero M, Missiaen R, Huang H, Bruning U, *et al*. (2017). The role of fatty acid beta-oxidation in lymphangiogenesis. Nature 542, 49–54.
Xiong J (2018a). Fatty acid oxidation in cell fate determination. Trends Biochem Sci 43, 854–857.
Xiong J (2018b). A 'Nobel' look at metabolism. Trends Endocrinol Metab 29, 809–813.
Xiong J, Kawagishi H, Yan Y, Liu J, Wells QS, Edmunds LR, Fergusson MM, Yu ZX, Rovira II, Brittain EL, *et al*. (2018). A metabolic basis for endothelial-to-mesenchymal transition. Mol Cell 69, 689–698 e687.
Xiong J, Todorova D, Su NY, Kim J, Lee PJ, Shen Z, Briggs SP, Xu Y (2015). Stemness factor Sall4 is required for DNA damage response in embryonic stem cells. J Cell Biol 208, 513–520.
Xu D, Zhao H, Jin M, Zhu H, Shan B, Geng J, Dziedzic SA, Amin P, Mifflin L, Naito MG, *et al*. (2020). Modulating TRADD to restore cellular homeostasis and inhibit apoptosis. Nature 587, 133–138.
Yun T, Ko HR, Jo DG, Park KW, Cho SW, Kim J, Ahn JY (2021). Inhibitor of DNA binding 2 (Id2) mediates microtubule polymerization in the brain by regulating alphaK40 acetylation of alpha-tubulin. Cell Death Discov 7, 257.
Zhou C, Jiang X, Liang A, Zhu R, Yang Y, Zhong L, Wan D (2020). COX10-AS1 facilitates cell proliferation and inhibits cell apoptosis in glioblastoma cells at post-transcription level. Neurochem Res 45, 2196–2203.